KSME

Springer

Journal of Mechanical Science and Technology 34 (1) 2020

Original Article
DOI 10.1007/s12206-019-1232-y

Keywords:
· CNC machine
· Spindle thermal error
· Thermal error compensation
· Dynamic gradient
· Unfalsified control

Correspondence to:
Zheng-chun Du
zcdu@sjtu.edu.cn

Citation:
Yao, X., Du, Z., Ge, G., Yang, J. (2020). Dynamic temperature gradient and unfalsified control approach for machine tool thermal error compensation. Journal of Mechanical Science and Technology 34 (1) (2020) 319-331.
http://doi.org/10.1007/s12206-019-1232-y

Received March 26th, 2019
Revised October 17th, 2019
Accepted November 1st, 2019

† Recommended by Editor
Hyung Wook Park

Dynamic temperature gradient and unfalsified control approach for machine tool thermal error compensation

Xiao-dong Yao, Zheng-chun Du, Guang-yan Ge and Jian-guo Yang

School of Mechanical Engineering, Shanghai Jiao Tong University, Shanghai, 200240, China

Abstract In this work, a novel machine tool thermal error modeling method based on dynamic temperature gradient is proposed, and a thermal error compensation method based on unfalsified control is developed. The dynamic temperature gradient is used to optimize the locations of temperature measuring points on the machine tool. Real-time compensation for the thermal error can be achieved using the developed compensation method by establishing the correlations between dynamic temperature gradient and thermal error in the machine tool. Different from traditional model-based methods, the developed compensation approach does not rely on an accurate model of the thermal error but instead uses online input/output data to adaptively select the best controller at any moment, thereby improving thermal error prediction accuracy and robustness. The effectiveness of the developed thermal error compensation method is demonstrated on a turning center, where the spindle thermal error is compensated during the manufacturing of 120 inner bore parts and 120 shaft parts. After compensation using the proposed approach, thermal errors are reduced from 27 μm to 9 μm for the inner bore parts and from 31 μm to 11 μm for the shaft parts, respectively.

1. Introduction

With increasing demands for high machining accuracy in precision and ultra-precision manufacturing, improving the thermal stability of CNC machine tools and reducing thermally induced errors have become the focus of research efforts [1]. Thermally induced errors are known to be the largest source of machining error in precision and ultra-precision manufacturing [2, 3]. Thermal errors can be reduced by means of the structural improvement of the machine tool through improved design, adopting machine components with high accuracy, and precise assembly of the machine. However, these approaches suffer limitations, such as high cost and difficulties in adapting to the various thermal conditions that occur with modern multipurpose CNC machine tools [3]. By contrast, thermal error compensation is not only cost-effective in reducing thermal errors but also adaptive to different thermal conditions associated with various machining tasks [1, 4].

Traditional thermal error compensation methods generally involve three steps, namely, measuring the temperature and thermal errors of the machine tool in typical operation conditions, establishing mathematical models correlating temperature in the machine tool with thermal errors, and compensating the thermal errors based on the established models [1]. In the last few years, researchers have proposed various methods to model and predict thermal errors of machining tools, which can be classified into three categories, namely, finite element method (FEM), mechanism analysis, and mathematical fitting methods.

Commercial software platforms are widely used for FEM. Huang [5] established an inverse method by a combination of CGM and ANSYS software to estimate the time-varying heat sources. Ma [6] considered thermal contact resistance and bearing stiffness and proposed a systematic modeling method of spindle thermal characteristics based on morphological characterization and mechanical properties. Brouwer [7] coupled FEM and discrete-element method

to establish a combined method for rotor bearings. The components of machine tool are simplified to build mathematical models for mechanism analysis method. Liu [8] proposed a power matching method considering the relationship between thermal errors and power inequality of spindle heat generation-dissipation. Zhang [9] considered the time-varying temperature of the environment and established the thermal error transfer function of the workpiece and the machine tools. Liu [10] established the radial thermal drift error model of different thermal postures for a machining tool and calculated the geometric parameters on the prediction results. The aforementioned types of modeling strategies can be classified as model-based prediction, which rely on an accurate model of the thermal error. However, the practical thermal error is dynamic and difficult to present in a mathematical model. Thus, data-driven prediction methods, such as backpropagation network [11], support vector machine [12], and fuzzy logistic [13], have been increasingly emphasized. A hybrid model [14, 15] that combines two or more different approaches has been proposed by some researchers.

Although thermal error compensation has obtained considerable development thus far, few compensation techniques can be effectively implemented in practical machining processes due to three major obstacles as follows. First, the numbers of temperature sensors and the optimal sensor locations are difficult to determine [16]. Optimal locations where local temperature is in approximately linear relationship with the thermal errors must be identified. The smallest number of temperature sensors necessary to capture the temperature field in the machine tool also needs to be identified to ensure fast compensation. Second, the detection and identification of the thermal characteristics of the machine tool can be time-consuming [1]. During the actual machining process, thermal errors are influenced by many factors, such as processing technologies, cutting parameters, cooling fluids, and ambient environment, resulting in nonlinear, quasi-static and pseudo-hysteric behaviors of thermal error. Hence, traditional thermal error modeling methods require simulation of the entire machining process under various conditions to detect and identify the machine tool thermal characteristics. On the basis of the statistical analysis of thermal error and temperature data, various modeling algorithms have been used to establish mathematical models to correlate machine tool temperature with thermal errors. The detection and identification process can be time-consuming and results in high cost in terms of production throughput. Third, the robustness of thermal error models is often poor [11]. The established mathematical model needs to accurately estimate the machine tool thermal errors under various complicated machining and environmental conditions. Therefore, the mathematical model should be able to adapt to the changes in the environment temperature and the variations of the thermal characteristics of the machine tool, which is difficult to achieve using traditional static or quasi-static mathematical models.

This study proposes a novel method for machine tool thermal error compensation based on unfalsified control (UC) theory applied to the spindle of a CNC turning center. Sec. 2 presents the theoretical and experimental analysis of spindle thermal deformation. Sec. 3 proposes an optimization strategy for the arrangement of the temperature measuring points. Sec. 4 presents the proposed thermal error compensation method, which can improve the robustness of thermal error compensation. Finally, Sec. 5 presents the experimental results.

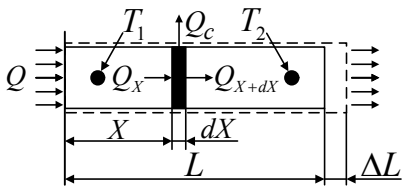

Fig. 1. One-dimensional simplified model of the spindle.

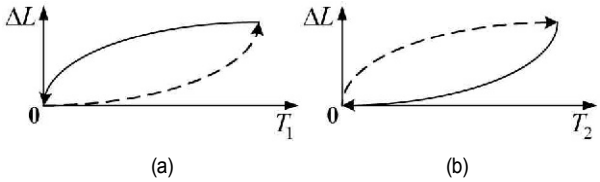

Fig. 2. Temperature-deformation relationship during warm-up (dashed line) and cool-down (solid line) stages.

2. Analysis of spindle thermal deformation

2.1 Theoretical analysis

Heat conduction in the spindle can be described by a one-dimensional simplified model, as shown in Fig. 1. Heat flux input Q comes from the fixed end at the left-hand side of the spindle and departs from the free end at the right-hand side. At the same time, heat exchange occurs between the spindle and the ambient environment through convection and radiation.

Temperature response dynamics to the heat flux input is dependent on the location of the temperature measuring point due to thermoelasticity [17]. As shown in Fig. 2(a), the measured temperature at T1 responds faster than the thermal deformation ΔL due to the location being closer to the heat source, whereas the measured temperature at T2 responds slower than the thermal deformation ΔL for being further away from the heat source flux input, as shown in Fig. 2(b). The further away the temperature measuring point from the heat source is, the longer the time delay present in the temperature response to the heat flux input will be. The pseudo-hysteric characteristic is illustrated in Fig. 2.

The thermal elongation of the spindle due to heat conduction can be expressed as follows:

$$\Delta L = \alpha \int_0^L \left[T(x) - T_0 \right] dx , \tag{1}$$

where α is the thermal expansion coefficient and can be con-

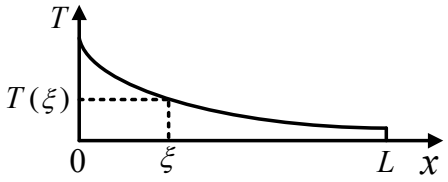

Fig. 3. Thermal deformation mode of spindle.

sidered a constant, L is the length of the spindle, $T(x)$ is the temperature at position *x*, and T_0 is the initial temperature of the spindle in thermal equilibrium. Applying the mean value theorem of integrals to Eq. (1) yields

$$T(\xi)-T_0=\frac{1}{L}\int_0^L\left[T(x)-T_0\right]dx\,, \tag{2}$$

where $T(\xi)$ is the mean value. ΔL can be described as follows:

$$\Delta L=\alpha L\left[T(\xi)-T_0\right], \tag{3}$$

where ξ is a certain position within the range of $[0,\ L]$ on the spindle, as shown in Fig. 3. Eq. (3) indicates that at least one point's temperature on the spindle can describe the thermal elongation ΔL of the spindle by itself, and the temperature $T(\xi)$ has a linear relationship with ΔL.

2.2 Experimental analysis

To detect the temperature field of the spindle, related experiments were conducted on an SMTCL ETC3650 NC center, which has a maximum rotational speed of 8000 rpm, a maximum machining diameter of 360 mm, and a FANUC 0i TD NC system. A total of four temperature sensors were attached on the machine tool, as shown in Fig. 4. The locations of the sensors are described as follows:

a) T1 was for measuring the temperature of the rear bearing;
b) T2 was for measuring the temperature of the front bearing;
c) T3 was for measuring the temperature of the front-end section; and
d) T4 was for measuring the environmental temperature.

A master ball was installed on the tool holder of the spindle, and a spindle rotational error tester was used to measure the spindle thermal error in the X-, Y-, and Z-directions.

The spindle was run at three sets of rotational speeds (i.e., 500, 1000, and 1500 rpm). Each experiment started from the condition of thermal equilibrium. The warm-up time was 120 min, and the sampling period was 10 s. During the entire procedure, temperature was measured at the selected sensor locations. The recorded readings are shown in Fig. 5. The thermal errors in the spindle in the X-, Y-, and Z-directions were measured simultaneously, as shown in Fig. 6.

Intrinsic connections between measured temperatures and thermal error could be observed. The correlation between

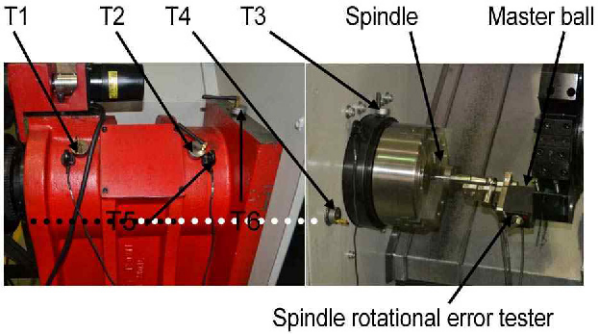

Fig. 4. Temperature sensor locations on the turning center.

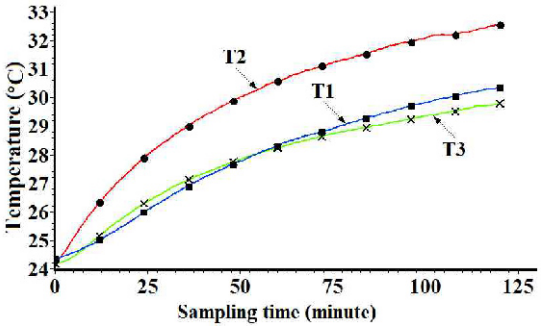

(a) 500 rpm

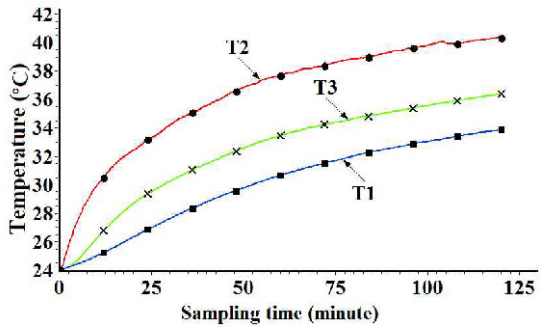

(b) 1000 rpm

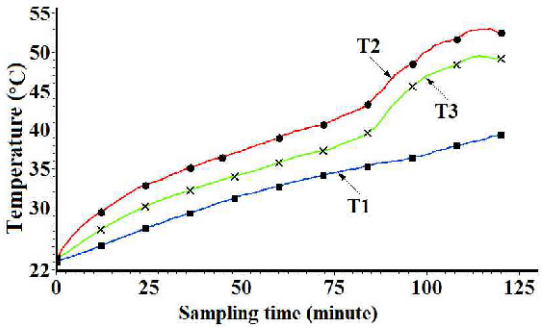

(c) 1500 rpm

Fig. 5. Temperature measured by three sensors at different rotational speeds.

measured temperatures at various sensor locations and thermal errors must be established at each rotational speed, which will be discussed in detail in the following subsections.

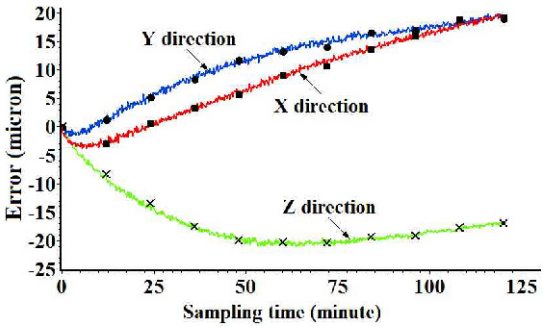

(a) 500 rpm

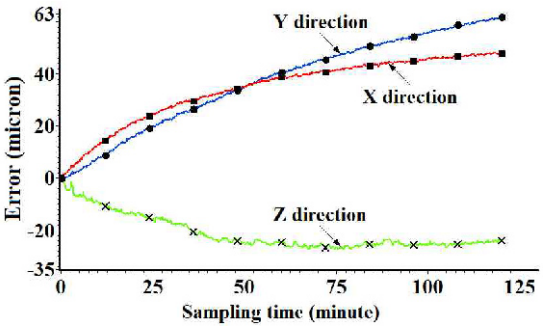

(b) 1000 rpm

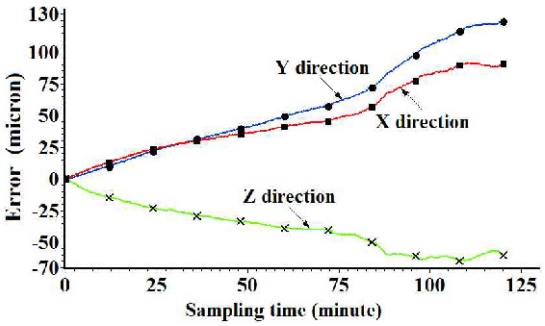

(c) 1500 rpm

Fig. 6. Thermal error recorded in the X-, Y-, and Z-directions at different rotational speeds.

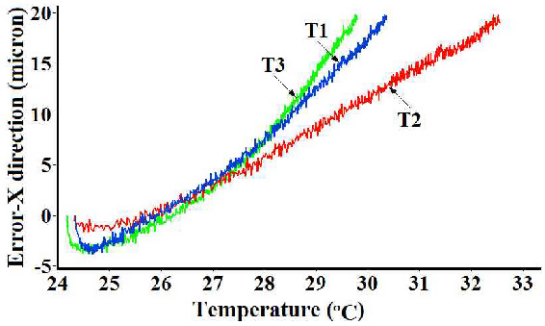

(a) Correlation curve between temperature values and thermal error in the X-direction

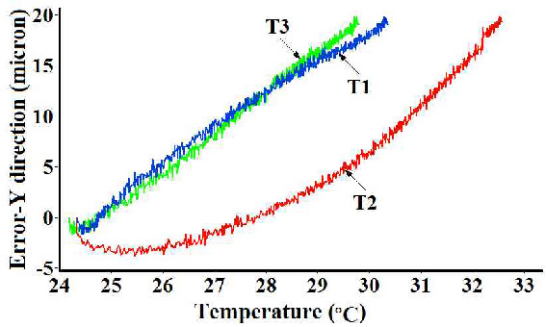

(b) Correlation curve between temperature values and thermal error in the Y-direction

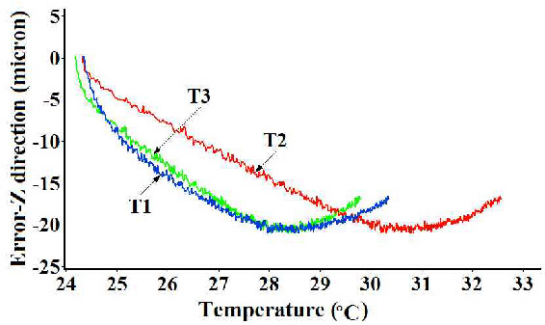

(c) Correlation curve between temperature values and thermal error in the Z-direction

Fig. 7. Correlation between temperature values and thermal error in three directions at rotational speed of 500 rpm.

2.2.1 Correlation between temperature and thermal error at 500 rpm rotational speed

The correlation between the thermal errors in the X-, Y-, and Z-directions and the measured temperatures are shown in Fig. 7. The temperature measured at T2 had an approximately linear relationship with the thermal error in the X-direction, whereas the temperatures measured at T1 and T3 lag the thermal error (Fig. 7(a)). The temperatures measured at T1 and T3 were in approximately linear relationship with the thermal error in the Y-direction, whereas the temperature measured at T2 was in advance of the thermal error (Fig. 7(b)). The temperature measured at all three locations at the behind part were in advance of the thermal error in the Z-direction, whereas the temperatures measured at T1 and T3 at the fore part lagged behind the thermal error, and the temperature measured at T1 at the fore part was in approximately linear relationship with the thermal error (Fig. 7(c)).

2.2.2 Correlation between temperature and thermal error at 1000 rpm rotational speed

Similarly, the correlations between measured temperatures and thermal errors at the rotational speed of 1000 rpm are summarized as follows.

Fig. 8(a)

a) T1: Lagged behind

b) T2 and T3: Approximately linear relationship

Fig. 8(b)

a) T1: Approximately linear relationship

b) T2 and T3: In advance

Fig. 8(c)

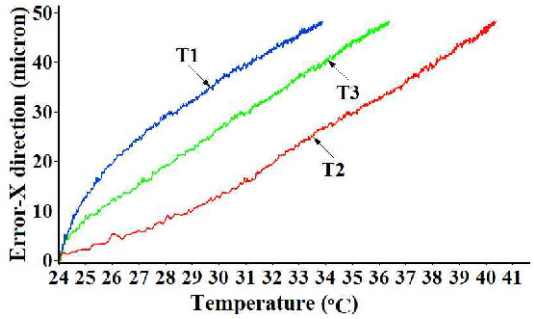

(a) Correlation between temperature values and thermal error in the X-direction

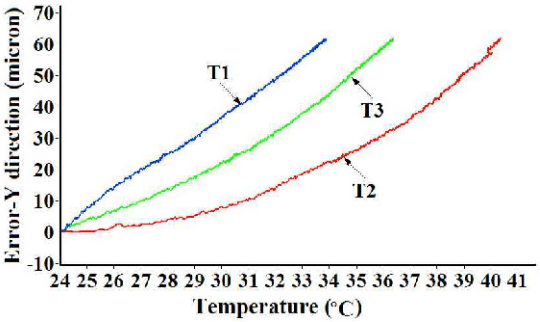

(b) Correlation between temperature values and thermal error in the Y-direction

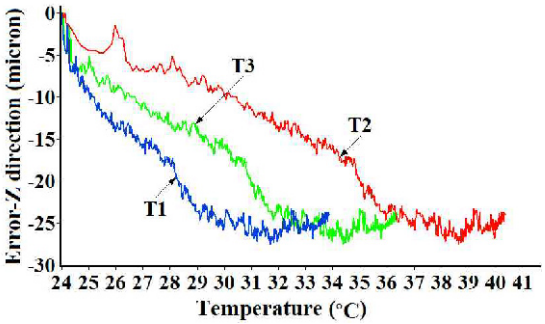

(c) Correlation between temperature values and thermal error in the Z-direction

Fig. 8. Correlation between temperature values and thermal error in three directions at rotational speed of 1000 rpm.

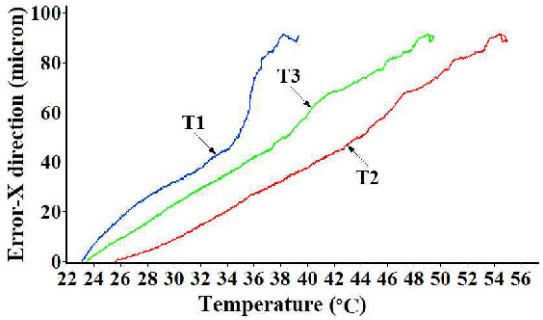

(a) Correlation between temperature values and thermal error in the X-direction

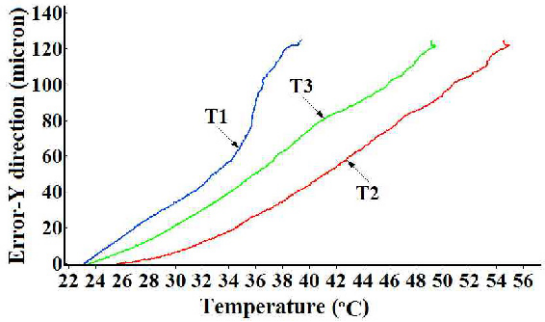

(b) Correlation between temperature values and thermal error in the Y-direction

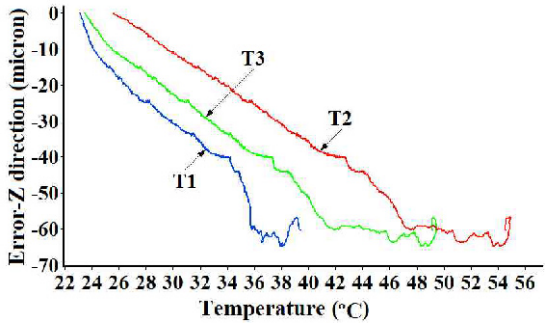

(c) Correlation between temperature values and thermal error in the Z-direction

Fig. 9. Correlation curve between temperature values and thermal error in three directions at rotational speed of 1500 rpm.

a) T1, T2, and T3 at the behind part: In advance
b) T1 and T3 at the fore part: Lagged behind
c) T2 at the fore part: Approximately linear relationship.

2.2.3 Correlation between temperature and thermal error at 1500 rpm rotational speed

Similarly, the correlations between measured temperatures and thermal errors at the rotational speed of 1500 rpm are summarized as follows.

Fig. 9(a)
a) T1: In advance
b) T2 and T3: Approximately linear relationship
Fig. 9(b)
a) T1: Lagged behind
b) T2: In advance
c) T3: Approximately linear relationship
Fig. 9(c)
a) T1 at the behind part: Lagged behind
b) T2 and T3 at the behind part: In advance
c) T1 and T3 at the fore part: Lagged behind
d) T2 at the fore part: Approximately linear relationship.

3. Optimization strategies for the arrangement of temperature measuring points

Due to thermal drift, radial and axial deviations are present in the spindle during the machining process. For turning centers, the radial deviation in the spindle has significant influence on

Table 1. Correlations between temperature at each measuring point and the spindle thermal error in the X-direction.

Correlation	T1	T2	T3
500 rpm	Lag	Approximate linearity	Lag
1000 rpm	Lag	Approximate linearity	Approximate linearity
1500 rpm	Advance	Approximate linearity	Approximate linearity

the machining precision. Hence, the thermal error in the X-direction can be regarded as the primary source of machining errors. The correlations between the measured temperatures at the measuring points and the thermal errors in the X-direction are shown in Table 1. This experimental result indicates that the optimal location for placing the measuring point is near the front bearing of spindle, whereas the temperature measured at T2 remains in approximately linear relationship with the spindle thermal error in the X-direction at all three spindle rotational speeds.

In practice, the tightness of assembly in the spindle affects the heat transfer rate of the bearings. Hence, even for the same type of spindles, the optimal location of the measuring point will vary as a result of the assembly process. Consequently, identification of the optimal locations of temperature measuring points based solely on the correlation between thermal error and measured temperature can be difficult and time-consuming under various operating conditions. To address these issues, an optimization strategy for temperature measuring points based on dynamic temperature gradient is proposed in this section. Correlation between the thermal error in the spindle and the temperature gradient under different heating conditions are analyzed.

3.1 Dynamic gradient of temperature sampling data

As previously mentioned, the temperature at T2 is in approximately linear relationship with the spindle thermal error at all three rotational speeds because the fore bearing is the main heat source in the spindle structure. In other words, the temperature at T2 responds to the thermal drift most quickly during the same sampling period. Here, the dynamic temperature gradient is used to establish a correlation with the spindle thermal error. The temperature measured at T2 at the rotational speed of 500 rpm is shown in Fig. 10, where $x(t)$ is set as the temperature sampling sequence and calculated in derivative by means of fourth-order central derivative method. Y_i is the sequence of the results after discrete differential calculation, as shown in Eq. (4).

The rotational speed is calculated as follows:

$$Y_i = \frac{1}{12dt}\left(-x_{i+2} + 8x_{i+1} - 8x_{i-1} + x_{i-2}\right), \quad (4)$$

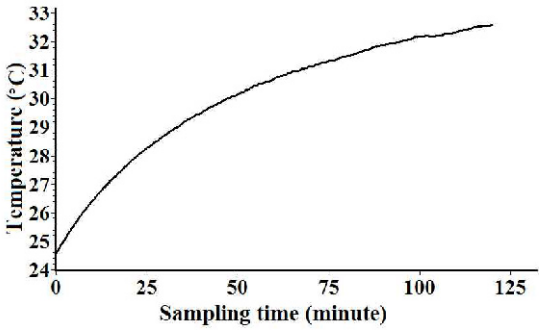

Fig. 10. Temperature statistical data of T2 at 500 rpm rotational speed.

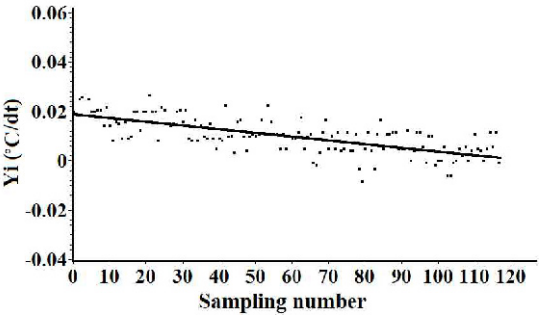

Fig. 11. Dynamic temperature gradient Y_i at measuring point T2.

where $i = 0,1,2,\cdots,n-1$, and n is the sampling size. x_{-2} and x_{-1} are the first and second elements are the first element of the initial conditions, respectively. x_n and x_{n+1} are the first and second elements of the final conditions, respectively.

Fig. 11 shows the Y_i values at each sampling moment, and the solid line is the linear fitting result for the Y_i sequence, as shown as follows:

$$Y_{500} = -5.7189 + 25.3362x\,. \quad (5)$$

The elements in the Y_i sequence are actually the values of temperature gradient in a unit sampling period. Thus, Y_i can be referred to as the dynamic gradient sequence of the temperature measuring point.

3.2 Correlation between dynamic temperature gradient and spindle thermal error

The measured thermal errors in the X-direction at the rotational speed of 500 rpm are shown in Fig. 12. The sequence of thermal errors has been resampled to filter the noise effect in the initial stage caused by instrument adjustment, and the sequence of thermal errors is calculated by polynomial fitting method. The fitting result is shown in Fig. 13.

As shown in Fig. 13, the distribution points are the thermal errors in the X-direction, and the solid line is the second-order polynomial fitting result, which can be described as follows:

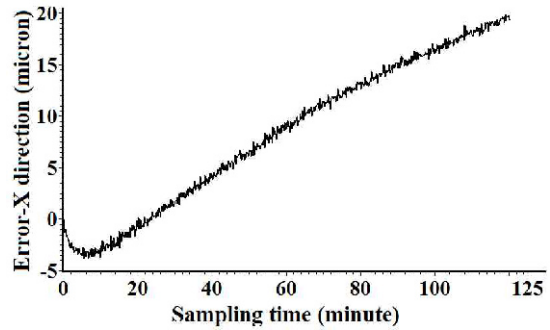

Fig. 12. Spindle thermal error in the X-direction at the rotational speed of 500 rpm.

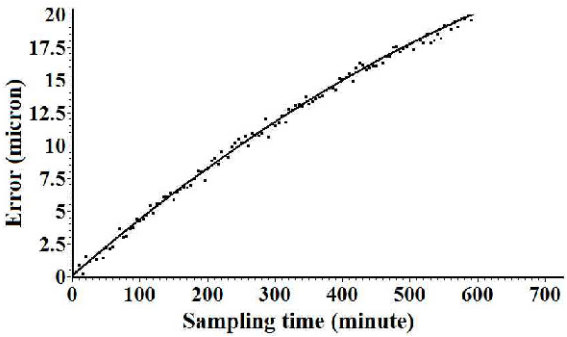

Fig. 13. Fitted curve of spindle thermal error in the X-direction.

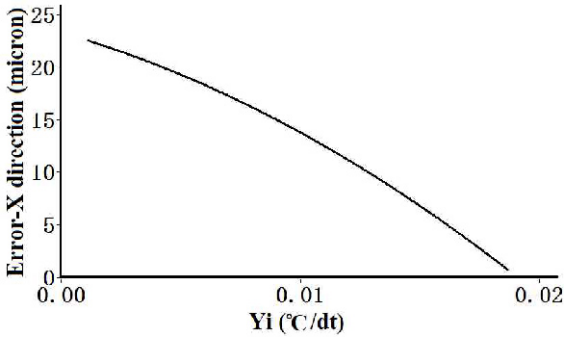

Fig. 14. Correlation between dynamic temperature gradient and thermal error in the X-direction.

$$\delta = 58.7962\times10^{-3} + 44.6941\times10^{-3}x - 18.6111\times10^{-6}x^2 . \quad (6)$$

The correlation between the dynamic temperature gradient at T2 and the thermal error is shown in Fig. 14. The dynamic temperature gradient is in approximately linear relationship with the thermal error, which indicates that the variation in the dynamic temperature gradient is synchronous with that in the spindle thermal error. Therefore, the thermal error can be estimated by monitoring the variations in the dynamic temperature gradient in real time.

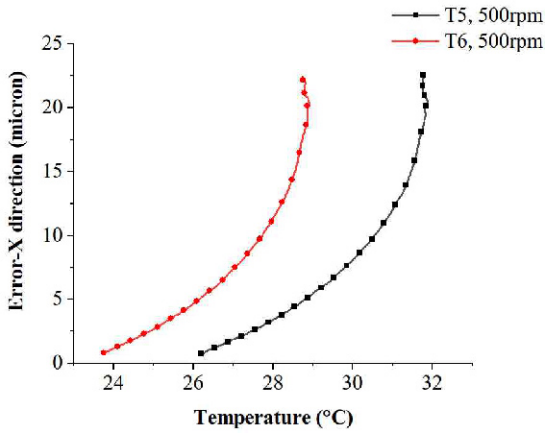

Fig. 15. Correlation between the temperatures at T5 and T6 and the thermal error at 500 rpm rotational speed.

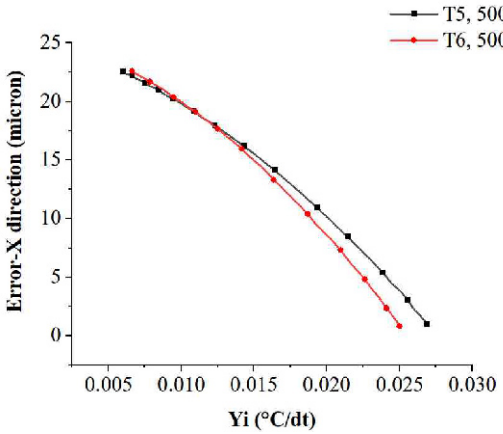

Fig. 16. Correlation between the dynamic temperature gradients at T5 and T6 and the thermal error at 500 rpm rotational speed.

3.3 Dynamic temperature gradient near the location of measuring point T2

Another two temperature sensors, namely, T5 and T6, are attached on the spindle near T2, as shown in Fig. 4. The spindle is run at the same three rotational speeds (i.e., 500, 1000, and 1500 rpm), and the temperature at T5 and T6, as well as the thermal errors, are measured. The correlations between dynamic temperature gradient and spindle thermal error are shown in Figs. 15-20 and compared in Table 2.

As shown in Table 2, the dynamic temperature gradients at T5 and T6 measuring points remain in approximately linear relationship with thermal error sequences at all three spindle rotational speeds.

3.4 Optimization strategies based on dynamic temperature gradient

The experimental results show that although the temperature at each measuring point has a nonlinear relationship with the spindle thermal error due to the different layout locations for

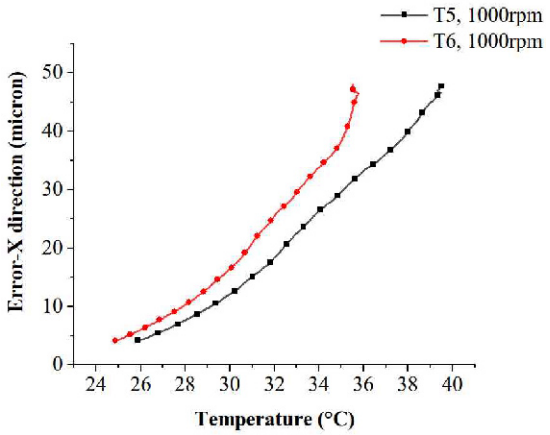

Fig. 17. Correlation between the temperatures at T5 and T6 and thermal error at 1000 rpm rotational speed.

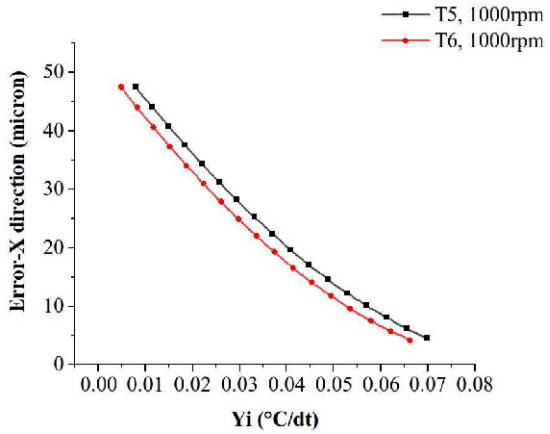

Fig. 18. Correlation between the dynamic temperature gradients at T5 and T6 and thermal error at 1000 rpm rotational speed.

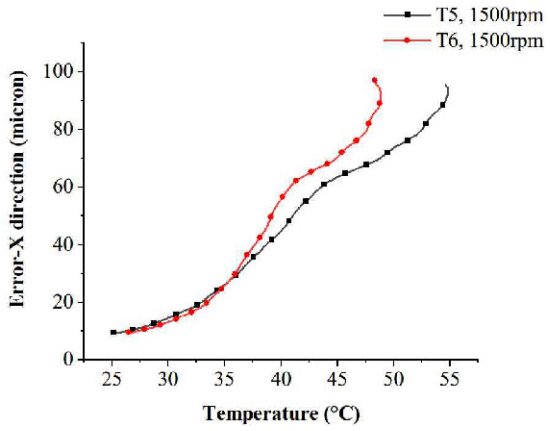

Fig. 19. Correlation between temperatures at T5 and T6 and thermal error at 1500 rotational speed.

measuring points and rotational speeds, the approximate relationship between the variation of the temperature field and the change in the spindle thermal error can still be found by calculating the dynamic temperature gradient values. On the basis

Table 2. Correlations between thermal error and temperature and between thermal error and dynamic temperature gradient.

Speed (rpm)	Correlation	T5	T6
500	Between thermal error and temperature	Nonlinearity	Nonlinearity
	Between thermal error and dynamic temperature gradient	Approximate linearity	Approximate linearity
1000	Between thermal error and temperature	Nonlinearity	Nonlinearity
	Between thermal error and dynamic temperature gradient	Approximate linearity	Approximate linearity
1500	Between thermal error and temperature	Nonlinearity	Nonlinearity
	Between thermal error and dynamic temperature gradient	Approximate linearity	Approximate linearity

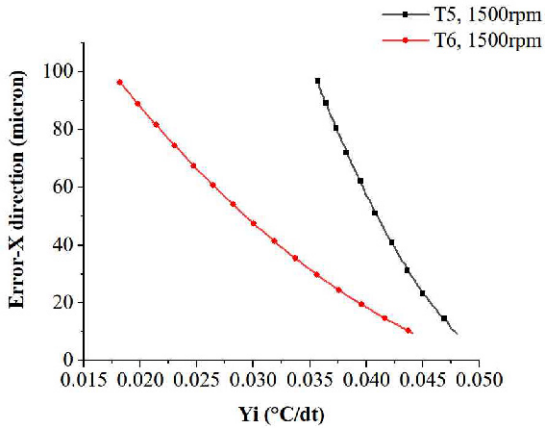

Fig. 20. Correlation between dynamic temperature gradients at T5 and T6 and thermal error at 1500 rpm rotational speed.

of the analysis of experimental results, the optimization strategies for the arrangement of the temperature measuring points can be summarized as follows.

(1) Multiple temperature sensors are placed near the fore and rear bearings, and the sensor location with the largest temperature variation during the test experiment is determined.

(2) The correlation between the spindle thermal error and the dynamic temperature gradient at the measuring points is constructed on the basis of the dynamic gradient of the temperature sampling sequence. If the correlation is approximately linear, then the measuring point can be considered as the optimal location to place the temperature sensor.

(3) If a linear correlation cannot be established, then the location of the measuring point can be slightly adjusted, and Steps 2 and 3 are repeated. This step is repeated until the correlation becomes approximately linear, and the measuring point can then be considered as the optimal location.

The optimization strategies can solve well the uncertainty problems demonstrated in the previous experimental analysis

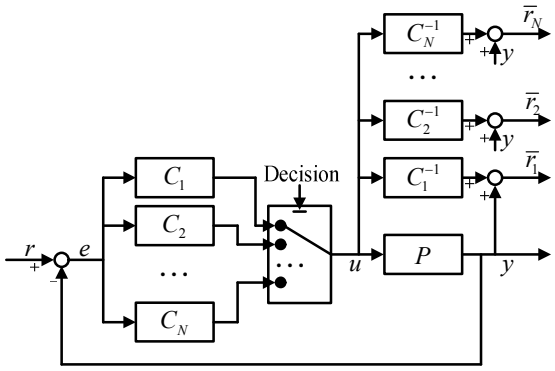

Fig. 21. Framework of UC method.

and have good robustness.

4. Thermal error modeling based on UC theory

On the basis of dynamic temperature gradient, UC theory is introduced into the online identification of the thermal characteristics of the spindle. Accordingly, a new modeling method for thermal error is proposed.

4.1 UC theory

The traditional control theory is a model building theory based on the hypothesis, which indicates that building the mathematical models for the controlled object must be based on some assumed conditions. However, these assumed conditions are often set based on the offline analysis of a set of previous sampling data from the controlled object. Hence, when the actual working conditions of the controlled object are different from these assumed conditions, the stability and robustness of the control model will often become poor. To solve this problem, UC theory [18-22] is presented in this study.

UC theory is a control method based on the online data driven control. UC method does not require building the traditional mathematical models. However, it can select the current controller from the candidate controller set, and the selected controller should be satisfied with the specific performance requirements. Hence, UC is essentially a switching control method. UC method works before the closed-loop feedback system and can effectively eliminate the pseudo controller.

As shown in Fig. 21, P is an unknown controlled object. The reversible and time-invariant controllers $C_1, C_2, \cdots, C_N$ belong to the given candidate controller set C, and the controller, which is used in the closed-loop feedback system, is a certain element in set C at any moment. At the current moment k, the previous input and output data $\{(u(\tau), y(\tau)) \mid \tau \in [0, k-1]\}$ of the controlled object, which are collected within the time interval $[0, k-1]$, are used to evaluate the controller $C_j, j = 1, 2, \cdots, N$. The controller with the optimal performance is selected as the controller at moment k. Notably, the performance of C_j must be evaluated before it is introduced into the closed-loop control system. The measurement data $u(\tau)$ and $y(\tau)$ are utilized to calculate the virtual reference signal $\bar{r}_j(\tau)$ of controller C_j, as shown in Eq. (7).

$$\bar{r}_j(\tau) = C_j^{-1}(u(\tau)) + y(\tau) \tag{7}$$

The control performance indicators $J(u, y, \bar{r}_j)$ and $(u(\tau), y(\tau), \bar{r}_j(\tau))$, $\tau \in [0, k-1]$ are used to evaluate controller C_j as shown in Eq. (8).

$$J_j(k) = J(u, y, \bar{r}_j(\tau), k) = \max_{\tau \in [0,k]} \frac{\|u(\tau)\|^2 + \|\bar{r}_j(\tau) - y(\tau)\|^2}{\|\bar{r}_j(\tau)\|^2 + \alpha} \tag{8}$$

In Eq. (8), $\alpha > 0$, and each $J_j(k)$, $j = 1, 2, \cdots, N$ is calculated. If $j^*(k) = \arg\min_{j=1,2,\cdots N} J_j(k)$, the controller acting on the closed-loop control system is considered to be $C_{j^*(k)}$ at each moment k. In other words, for UC method, the other $N-1$ numbers of pseudo controllers are eliminated, except for $C_{j^*(k)}$ at each moment k. The non-pseudo controller $C_{j^*(k)}$ is used to act on the closed-loop control system.

During the process of UC, a switching mechanism is necessary for selecting an appropriate controller to replace the controller that cannot meet the performance indicators. Hence, all the controllers in the set should be examined, and only the controller that meets the performance indicators can be introduced into the closed-loop control system.

4.2 Application of UC in thermal error compensation

UC consists of two elements as follows:

a) A candidate controller set composed of reversible controllers, and

b) a performance indicator for evaluating the controllers.

The spindle thermal errors have strong nonlinear characteristics, such as being quasi-static and pseudo-hysteric. Hence, ensuring the accuracy and robustness of the controller can be difficult for the traditional mathematical model. However, on the basis of UC theory, the performance of the controllers can be evaluated online according to the real-time operating conditions, and the optimal controller will be self-adaptively switched and introduced into the control loop. Consequently, the UC method has a strong applicability to solve nonlinear problems, such as spindle thermal errors.

4.2.1 Candidate controller set for spindle thermal error compensation

For thermal error compensation, the candidate controller set should be initially established. Here, T5 is selected as the temperature measuring point. On the basis of the correlation between dynamic temperature gradients and thermal errors shown in Figs. 16, 18 and 20, the mathematical expressions of

the thermal error compensation controllers at different rotational speeds are described in Eqs. (9)-(11), respectively.

$$\delta_{500} = -1.032\times10^{3}\Delta G + 19.8648\,, \tag{9}$$

$$\delta_{1000} = -5.9044\times10^{3}\Delta G + 46.4441\,, \tag{10}$$

$$\delta_{1500} = -7.0257\times10^{3}\Delta G + 340.4407\,, \tag{11}$$

where δ_{500}, δ_{1000}, and δ_{1500} are the thermal errors at different speeds, and ΔG is the corresponding dynamic gradients of T5. The scope of the candidate controller set can be further extended using additional temperature and thermal error data. The candidate controller set involved here is a group of linear functions that describe the correlation between thermal error and dynamic temperature gradient, which can be expressed as follows:

$$\delta_v = k\Delta G + b\,, \tag{12}$$

where δ_v is the thermal errors at speed *v*, *k* is the correlation between dynamic temperature gradients and thermal errors, *ΔG* is the corresponding dynamic gradients, and *b* is the intercept.

4.2.2 Performance indicator for controller evaluation

The performance indicator for evaluating the controllers is confirmed according to the measured input/output (I/O) data of the controlled object. The output data of the controller for the spindle thermal error compensation are the sampled temperature at the measuring point, and the input data are actually only the sampling time series. Thus, the performance indicator for evaluating the controllers can be set based on the dynamic temperature gradient values. As shown in Fig. 11, Y_i is the dynamic gradient sequence at the rotational speed of 500 rpm. The residual error sequence after linear fitting is shown in Fig. 22, and the mean square error of the fitting function is equal to 0.0000267. Similarly, the fitting functions of Y_i at 1000 rpm and 1500 rpm are described in Eqs. (13) and (14).

$$Y_{1000} = 5.1216\times10^{-2} - 9.0414\times10^{-5}x \tag{13}$$

$$Y_{1500} = 4.8081\times10^{-2} - 1.7799\times10^{-5}x \tag{14}$$

In both cases, the mean square errors of fitting functions are 0.0000922 and 0.0000838.

The performance indicator can be acquired as follows. The sampling period is set to t, and $T=\{T_1,T_2,\cdots T_n\}$ is the temperature sampling sequence at the sampling moment n. From the third sampling moment, T is determined using fourth-order central derivative (see Eq. (8)), and the discrete dynamic temperature gradient sequences dT are fitted synchronously, as shown as follows

$$dT = K_n t_n + B_n\,, \tag{15}$$

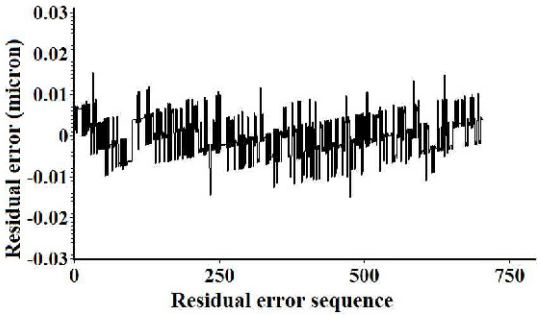

Fig. 22. Residual error sequence of dynamic gradient linear fitting.

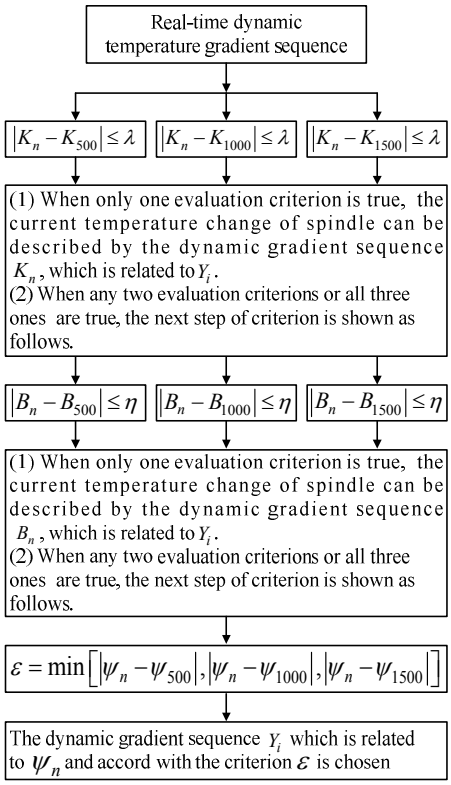

Fig. 23. Flow diagram of the criterion of performance indicator for UC.

where K_n is the slope of the fitting function at the sampling moment n; B_n is the intercept of the fitting function; t_n is the sampling time sequence; and ψ_n is used as the mean square error of the fitting function.

The switching mechanism of the performance indicator for evaluating the controllers can be described by the flow diagram in Fig. 23.

λ is set as the slope determination factor, and η is the intercept determination factor. ε is the mean square error determination factor. Thus, for the finite candidate controller set of the thermal error compensation, all the determination factors should be examined during the process of eliminating the pseudo controllers and selecting the applicable controller. Finally, the optimal controller is identified and applied to the current thermal error compensation.

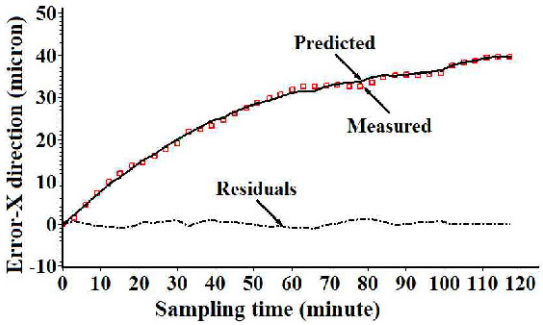

Fig. 24. Comparison of measured system output and the predicted output for spindle thermal error based on UC.

Furthermore, the candidate controller set above is only based on three sets of rotational speeds. For the practical application, the number of the thermal error compensation controllers and the performance indicators of dynamic temperature gradient at different rotational speeds can be extended, which makes the UC method for the thermal error compensation accurate and robust.

4.2.3 Verification of prediction accuracy for thermal error based on UC method

An experiment was conducted on the same turning center to verify the prediction accuracy of the UC method. Temperature sensor T6 was considered as the measuring point, and the spindle is run at the rotational speed of 1500 rpm.

The measured thermal errors are shown by the red points in Fig. 24, whereas the predicted errors are shown in solid line. The dotted line shows the residual errors in the prediction. The variation range of measured values is [0 μm, 39.6 μm], and the range of residual error is [−1.2 μm, 1.2 μm]. In this experiment, 96.97 % of the maximum error range of the thermal deformation can be predicted. Online prediction for the spindle thermal error based on UC is achieved, and the prediction accuracy is excellent.

5. Experimental results

Another experiment was performed to compensate the thermal error in the X-direction during the machining process of parts, as shown in Fig. 25. The spindle was run at six sets of rotational speeds for 120 min. Temperature at T6 was measured, as shown in Fig. 26.

The performance indicators were calculated based on the dynamic temperature gradients, and the controller based on the UC method was applied to the machining process to compensate the thermal error in real time. The calculated results about the slope and intercept determination factors of the fitting functions are shown in Table 3.

Two groups of 60 inner bore parts each were machined with and without compensation of the spindle thermal error, starting from the initial thermal equilibrium status. The inner diameter of the inner bore part is the most representative and requires the highest tolerances; thus, it is measured to test the compensation result. The inner bore part has a nominal diameter of 32.815 mm, and the upper and lower tolerance limits are 32.825 mm and 32.800 mm, respectively. The inner diameters of the 120 machined parts are shown in Fig. 27. Without thermal error compensation, the inner diameter ranged between 32.788 mm and 32.814 mm, and the maximum error was 27 μm. Less than 1/3 of the parts were machined within the tolerance limits. When thermal error compensation was applied, the inner diameter of the machined parts ranged between 32.807 mm and 32.815 mm. The maximum error was 9 μm, and 100 % of the parts were within tolerance limits, indicating that the inner diameter errors were effectively controlled.

Similarly, the external diameter of the shaft part requires the highest tolerance; thus, it is measured to test the compensation results. The external diameter of 120 shaft parts machined with

Table 3. Determination factors of fitting functions of the dynamic gradient.

Rotational speed (rpm)	Slope	Intercept
500	−3.1346E-5	0.02063
1000	−5.1043E-5	0.00327
1500	−7.5064E-5	0.03765
2000	−9.0936E-5	0.04503
2500	−2.9916E-4	0.04705
3000	−5.5646E-4	0.05437

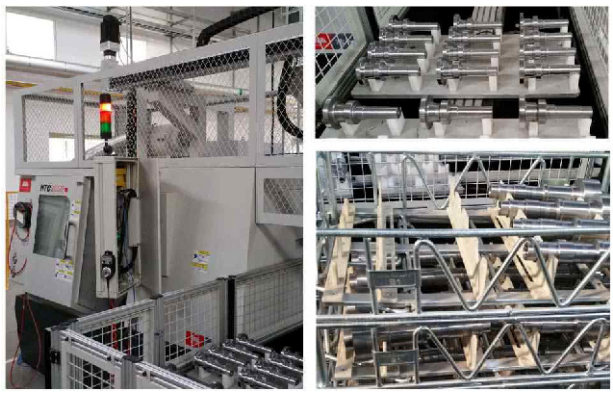

Fig. 25. Thermal error compensation for practical machining.

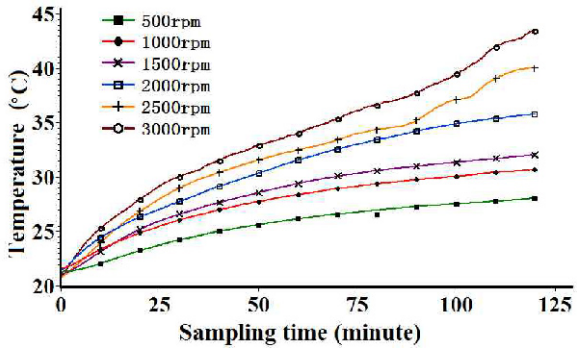

Fig. 26. Temperature at T6 at six sets of rotational speeds.

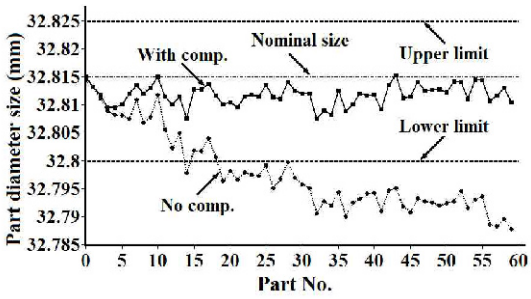

Fig. 27. Statistical results about the inner diameters of processed parts.

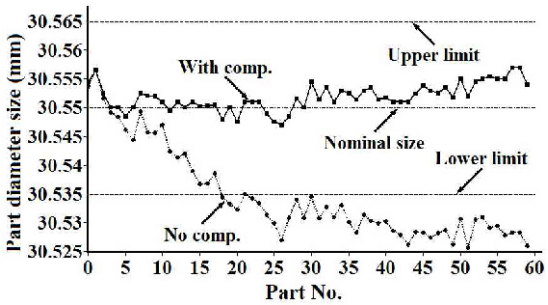

Fig. 28. Statistical results about the external diameter of processed parts.

and without thermal error compensation are shown in Fig. 27. The shaft part has a nominal external diameter of 30.550 mm, and an upper and lower tolerance limit of 30.565 mm and 30.535 mm. Without spindle thermal error compensation, the external diameter of the 60 machined parts ranged between 30.526 mm and 30.557 mm, and the maximum error was 31 μm. Less than 1/3 of the parts were machined within the tolerance limits. When thermal error compensation was applied, the external diameter of the machined parts ranged between 30.547 mm and 30.557 mm. The maximum error was 11 μm, and all machined parts were well within tolerance limits.

Both experiments demonstrated the effectiveness of the prediction and compensation of the thermal error in the spindle based on UC theory.

6. Conclusions

Thermal error has always been a key issue in the precision enhancement of machine tools for tool builders and users. In this study, a systemic solution for thermal error compensation was proposed, and careful research work was performed. First, a novel dynamic temperature gradient method was proposed to optimize the locations of temperature measuring points on the machine tool. The temperature fields were detected through the correlation between temperatures at three measuring points and thermal error rotational speeds of 500, 1000, and 1500 rpm, as shown in Figs. 7-9, respectively. Then, the dynamic temperature gradient values of two measuring points were calculated, as shown in Figs. 15-20, to ensure the linear relationship between the variation of the temperature field and the change in the spindle thermal error. Furthermore, a spindle thermal error compensation method was developed based on UC theory using the dynamic temperature gradient at the optimal sensor location. The effectiveness of this compensation method was demonstrated using two practical part manufacturing experiments. The experimental results indicated that the thermal errors were reduced from 27 μm to 9 μm for the inner bore parts and from 31 μm to 11 μm for the shaft parts.

The advantages of the proposed compensation method are as follows. (1) Strong robustness. The developed approach does not rely on an accurate model of the thermal error, but instead uses online I/O data to adaptively select the best controller at any moment, thereby improving thermal error prediction accuracy and robustness. (2) High efficiency. The dynamic temperature gradient is proposed to identify the relationship between temperature and thermal errors, which greatly shortened the identification time for the optimal location of measuring points. (3) After the identification of the measuring point, only few temperature sensors are required. Therefore, this compensation method shows great engineering capacity to reduce thermal error and the potential for further application to various types of machine tool.

Acknowledgments

This research was sponsored by the National Key R&D Program of China (No. 2018YFB1701204), National Natural Science Foundation of China (No. 51975372), and Shanghai Civil-Military Integration Project (No. 2016-63).

References

[1] Y. Li et al., A review on spindle thermal error compensation in machine tools, *Int. J. Mach. Tools Manuf.,* 95 (2015) 20-38.

[2] J. Bryan, International status of thermal error research, *Annals of the CIRP*, 39 (2) (1990) 645-656.

[3] M. Weck and P. M. Keown, Reduction and compensation of thermal error in machine tools, *Annals of the CIRP*, 44 (2) (1995) 589-598.

[4] J. Yang, J. Yuan and J. Ni, Thermal error mode analysis and robust modeling for error compensation on a CNC turning center, *Int. J. Mach. Tools Manuf.*, 39 (1999) 1367-1381.

[5] J. H. Huang, T. T. Ngo and C. C. Wang, An inverse method for estimating heat sources in a high speed spindle, *Appl. Therm. Eng.*, 105 (2016) 65-76.

[6] C. Ma et al., Simulation and experimental study on the thermally induced deformations of high-speed spindle system, *Appl. Therm. Eng.*, 86 (2015) 251-268.

[7] M. D. Brouwer et al., Combined explicit finite and discrete element methods for rotor bearing dynamic modeling, *Tribol. Trans.*, 58 (2) (2015) 300-315.

[8] T. Liu et al., Power matching based dissipation strategy onto spindle heat generations, *Appl. Therm. Eng.,* 113 (2017) 499-507.

[9] C. Zhang, F. Gao and L. Yan, Thermal error characteristic analysis and modeling for machine tools due to time-varying

environmental temperature, *Precis. Eng.,* 47 (2017) 231-238.
[10] K. Liu et al., Modeling and compensation for spindle's radial thermal drift error on a vertical machining center, *Int. J. Mach. Tools Manuf.*, 105 (2016) 58-67.
[11] X. Zhu, S. Xiang and J. Yang, Novel thermal error modeling method for machining centers, *Proc. Inst. Mech. Eng. Part C J. Mech. Eng. Sci.*, 229 (8) (2015) 1500-1508.
[12] J. Yang et al., Thermal error modeling and compensation for a high-speed motorized spindle, *Int. J. Adv. Manuf. Technol.*, 77 (5-8) (2015) 1005-1017.
[13] J. Yang et al., Thermal error compensation on a computer numerical control machine tool considering thermal tilt angles and cutting tool length, *Proc. Inst. Mech. Eng. Part B J. Eng. Manuf.,* 229 (1) (2015) 78-97.
[14] Y. Zhang, J. Yang and H. Jiang, Machine tool thermal error modeling and prediction by grey neural network, *Int. J. Adv. Manuf. Technol.,* 59 (9-12) (2012) 1065-1072.
[15] S. Xiang, H. Lu and J. Yang, Thermal error prediction method for spindles in machine tools based on a hybrid model, *Proc. Inst. Mech. Eng. Part B J. Eng. Manuf.,* 229 (1) (2015) 130-140.
[16] H. Liu, E. Miao, X. Zhuang and X. Wei, Thermal error robust modeling method for CNC machine tools based on a split unbiased estimation algorithm, *Precision Engineering,* 51 (2018) 169-175.
[17] Y. Hong and N. Jun, Dynamic modeling for machine tool thermal error compensation, *Journal of Manufacturing Science and Engineering*, 5 (125) (2003) 245-254.
[18] H. J. Pahk and S. W. Lee, Thermal error measurement and real time compensation system for the CNC machine tools incorporating the spindle thermal error and the feed axis thermal error, *Int. J. Adv. Manuf. Technol.,* 20 (7) (2002) 487-494.
[19] J. Helvoortvan, B. Jagerde and M. Steinbuch, Direct data-driven recursive controller unfalsification with analytic update, *Automatica*, 43 (12) (2007) 2034-2046.
[20] J. Helvoortvan, B. Jagerde and M. Steinbuch, Data-driven multivariable controller design using ellipsoidal unfalsified control, *Systems and Control Letters*, 57 (9) (2008) 759-762.
[21] G. Battistelli et al., Stability of unfalsified adaptive switching control in noisy environments, *IEEE Transactions on Automatic Control,* 55 (10) (2010) 2424-2429.
[22] S. Baldi et al., Multi-model unfalsified adaptive switching supervisory control, *Automatica*, 46 (2) (2010) 249-259.

Zheng-chun Du is an Associate Professor at the School of Mechanical Engineering, Shanghai Jiao Tong University, Shanghai, China. He received his Ph.D. in Mechanical Engineering from Southeast University. His research interests include error measurement, modeling, and compensation of machine tools, precision measurement, and processing.